Dalton Transactions

ROYAL SOCIETY OF CHEMISTRY

PAPER

View Article Online
View Journal | View Issue

Cite this: *Dalton Trans.*, 2026, **55**, 5266

Transition metal complexes with phosphine oxide appended aza-macrocycles – effects of ring size and denticity

Julie M. Herniman,[a] George P. Keeling,[b] Rhys P. King,*[a] Mark E. Light,[a] Navya Kandathil Sintho,[a] Kate Snowsill[a] and Gillian Reid*[a]

Two new phosphine oxide appended aza-macrocyclic ligands, $\mathbf{L^1}$ and $\mathbf{L^3}$, have been prepared in good yield from the reaction of Bn-tacn and Bn-cyclen (tacn = 1,4,7-triazacyclononane; cyclen = 1,4,7,10-tetraazacyclododecane) with paraformaldehyde and diphenylphosphine oxide. They are characterised spectroscopically and *via* a crystal structure determination for $\mathbf{L^3}$·MeCN. The coordination chemistry of these ligands and the known **NOTP-Ph** ($\mathbf{L^2}$) with divalent late 3d metal ions, Co, Ni, Cu and Zn, has been investigated, showing that $\mathbf{L^1}$ and $\mathbf{L^2}$ bind in a pentadentate and hexadentate manner, respectively, in all cases. The potentially heptadentate $\mathbf{L^3}$ is found to coordinate to Co(II) and Zn(II) in a hexadentate manner (N_4O_2 donor set) giving distorted trigonal prismatic cations, and to Ni(II) through the same N_4O_2 donor set, but in a distorted octahedral geometry. These assignments follow from a combination of elemental analyses, mass spectrometry, IR, UV-visible, ^{1}H and ^{31}P{^{1}H} NMR spectroscopic data, as appropriate, and X-ray crystal structures of several representative examples incorporating $\mathbf{L^1}$–$\mathbf{L^3}$. The properties of the new complexes are also compared to the literature data from the corresponding complexes of the cyclen macrocycle bearing four diphenylphosphine oxide pendant groups, **DOTP-Ph**, which are distinctly different. Overall, these studies across this series of ligands and metals demonstrate that the macrocyclic ring size, metal ion type and the number of pendant phosphine oxide arms all play an important role in determining the resulting coordination numbers and geometries.

Received 30th January 2026,
Accepted 28th February 2026

DOI: 10.1039/d6dt00255b

rsc.li/dalton

Introduction

Phosphine oxides are a very widely studied, versatile and tuneable class of ligands, forming stable complexes with elements from across the s-, p-, d- and f-block,[1–3,4,5] and with applications in catalysis,[6] separation science[7] and medicinal chemistry.[8] While there have been numerous studies focussed on simple monodentate and chelating bi-/poly-dentate phosphine oxides, macrocyclic ligands bearing phosphine oxide pendant arms have received much less study, although they might be expected to be superior ligands due to their macrocyclic core.

A small number of phosphine oxide appended macrocycles have been reported.[9,10] **NOTP-Ph** ($\mathbf{L^2}$), first described by Scherbakov and co-workers, was obtained by the reaction of tacn (1,4,7-triazacyclononane), paraformaldehyde, and diphenylphosphine oxide in benzene at 140 °C. **NOTP-Ph** ($\mathbf{L^2}$) (Scheme 1), with its N_3O_3-donor set, was reported to form stable complexes with group 1^2 and group 2^1 ions in organic solvents. Characterisation data was very limited, however, conductivity data on 1 : 1 complexes of $\mathbf{L^2}$ with alkali metal 2,4-dinitrophenolates were reported to follow the trend Li > Na > K > Cs, while the reactions of $\mathbf{L^2}$ with CaI_2 and MgI_2 yielded products of apparent composition $(MgI_2)_3(\mathbf{L^2})_2{\cdot}H_2O$ and $Ca(\mathbf{L^2})I_2{\cdot}3H_2O$, respectively, although their structures remain unknown. The only reported transition metal complex of $\mathbf{L^2}$ was with cobalt thiocyanate, and suggested that compounds with various compositions can form depending on the metal : ligand ratio, including products that were tentatively formulated as $[(Co(NCS))_2(\mu\text{-}\mathbf{L^2})]_2[Co(NCS)_4]{\cdot}NCS$ (blue) and $[Co(NCS)_2(\mathbf{L^2})]$ (pink), on the basis of UV-vis data.[11,12]

More recently, some chemistry of the potentially octadentate cyclen derivative (cyclen = 1,4,7,10-tetraazacyclododecane), **DOTP-Ph**, has been reported with a range of hydrated divalent 3d metal perchlorates (M = Co, Ni, Cu, Zn), also showing that the coordination environment is metal dependent, with Cu(II) giving a five-coordinate complex with an N_4O donor set and both cobalt and zinc giving unusual eight-coordinate complexes with octadentate coordination (N_4O_4 donor sets).[13] In 2023, Troadec *et al.* reported two new chelators based on the cyclam core (cyclam = 1,4,8,11-tetraazacyclotetradecane) with either one or two $-CH_2P(O)Ph_2$ pendant arms and demon-

[a]*School of Chemistry and Chemical Engineering, University of Southampton, Southampton SO17 1BJ, UK. E-mail: R.P.King@soton.ac.uk, G.Reid@soton.ac.uk*
[b]*GE HealthCare, Pollards Wood, Nightingales Lane, Chalfont St Giles, Bucks, HP8 4SP, UK*

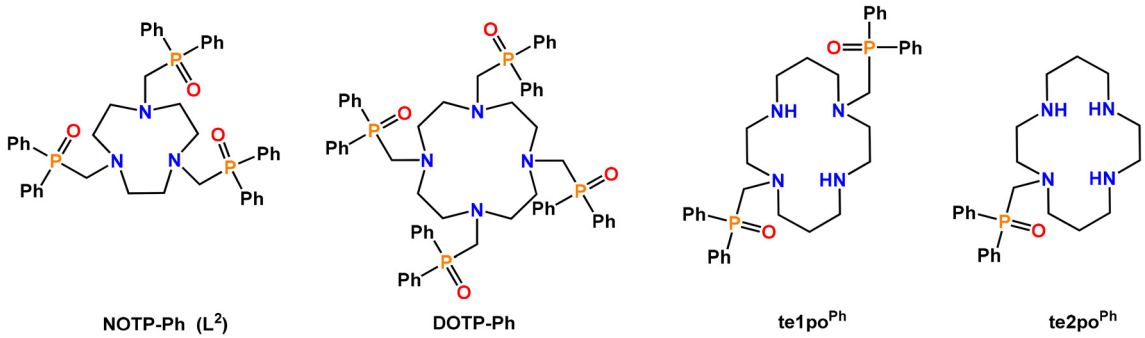

Scheme 1 Previously reported aza-macrocyclic ligands with phosphine oxide pendant arms.

strated for ligand **te1po^{Ph}** that judicious choice of ring-size and pendant arm allows for a copper(II)-specific chelator.[14] However, there have been no systematic studies on the coordination chemistry of phosphine oxide functionalised aza-macrocycles varying both the chelator and metal ion.

We describe here the syntheses of three phosphine oxide appended aza-macrocycles derived from either the tacn or cyclen core and offering different donor sets and ring sizes. Their coordination chemistry is then explored with four divalent 3d transition metal ions (Co^{2+}, Ni^{2+}, Cu^{2+}, Zn^{2+}), with spectroscopic and X-ray crystallographic data showing that both the metal and the ligand type are important in determining the structural outcome. The new ligands and complexes have been characterised by IR, UV-visible and ^{1}H NMR spectroscopy, as appropriate, mass spectrometry, and full X-ray crystal structure analyses are described for **L^3** and for 10 representative complexes incorporating **L^1**–**L^3**.

Results and discussion

Two new ligands, **BnNODP-Ph** (**L^1**) and **BnDOTP-Ph** (**L^3**) were synthesised by the reaction of Bn-tacn or Bn-cyclen with paraformaldehyde and diphenyl phosphine oxide (Scheme 2). The (known) **NOTP-Ph** (**L^2**) was prepared similarly from tacn, avoiding the use of the benzene solvent in the reported method.[2] The ^{31}P{^{1}H} NMR spectra of **L^1** and **L^2** each ligand shows singlet resonances at +27.8 and +26.0 ppm, respectively, *i.e.* to high frequency from H(O)PPh_2 (21.5 ppm);[15] **L^3** shows two distinct phosphorus environments at +27.4 and +27.6 ppm in a 1 : 2 ratio, respectively. All three ligands show peaks at around 1175 cm^{-1} in their IR spectra, attributed to the P═O stretch from the phosphine oxide arms.

Crystals of an acetonitrile solvate of **L^3** (**L^3**·MeCN) were grown from a saturated solution of the ligand in MeCN, with the ligand present in its free-base form (Fig. 1(a)). The P═O bond lengths are identical within error (~1.49 Å) and are typical for uncoordinated phosphine oxides. There are close contacts between the P═O groups and CH's of the cyclen ring, which might direct the conformation of the ligand in the solid state, these are shown in Fig. 1(b). The benzyl group is found below the cyclen N_4 ring, while two phosphine oxide arms (P1 and P2) lie approximately in the N_4-plane and the P3 arm lies above the N_4-plane.

Complexes of **L^1**–**L^3** were synthesised by reacting the appropriate divalent 3d metal nitrate hydrate with the ligand in methanol, followed by the addition of an excess of Na[BPh_4] (for all except copper) to provide a large, non-coordinating anion for charge balance and to encourage precipitation of the target complexes. The isolated [BPh_4]$^-$ salts were recrystallised from MeCN. For copper(II) it was found that the complexes formed as [$Cu(NO_3)_4$]$^{2-}$ salts, hence instead, a 2 : 1 stoichiometric ratio $Cu(NO_3)_2{\cdot}3H_2O$:ligand was reacted with the ligands to isolate the complexes.

For **L^1**, the Cu(II) complex was isolated as a blue-green solid, the Zn(II) complex as a colourless solid, while the Co(II) and Ni(II) complexes were isolated as light pink and green complexes, respectively. Their UV-vis data are consistent with six-coordination, and microanalysis also confirmed the formulation to be [M(**L^1**)(MeCN)][BPh_4]$_2$ for all except M = Cu. The ^{1}H and ^{31}P{^{1}H} NMR spectra of the Zn(II) complex are also consistent with the formulation [Zn(**L^1**)(MeCN)][BPh_4]$_2$ with the latter showing a singlet at 35.9 ppm, significantly to high frequency from **L^1** (+27.7), indicating coordination of both pendant arms. The IR spectra of [M(**L^1**)(MeCN)][BPh_4]$_2$ (M = Co, Ni, Zn) are essentially identical, with a peak at 1139 cm^{-1} assigned to the coordinated P═O and the absence of the original peak at 1179 cm^{-1} in **L^1** itself.

Crystals of [Cu(**L^1**){$Cu(NO_3)_4$}] were grown by diffusion of diethyl ether into an acetonitrile solution of the complex. The crystal structure of the cation is shown in Fig. 2(a) below, with the Cu(II) of the cation in a six-coordinate environment with a distorted Jahn–Teller elongated octahedral geometry along the N1–Cu1–O3 axis. The [$Cu(NO_3)_4$]$^{2-}$ dianion interacts weakly with the copper in the cation, with a Cu1–O3 bond distance of 2.5602(11) Å, much longer than the Cu–O bonds involving the phosphine oxide functions (1.9745(9) and 1.9823(9) Å), but this is clearly still sufficient to out-compete coordination by the MeCN.

Diffusion of Et_2O into MeCN solutions of the other metal complexes of **L^1** led to the crystals of the salts, [M(**L^1**)(MeCN)][BPh_4]$_2$ (M = Co, Ni, Zn); the structure for M = Co is

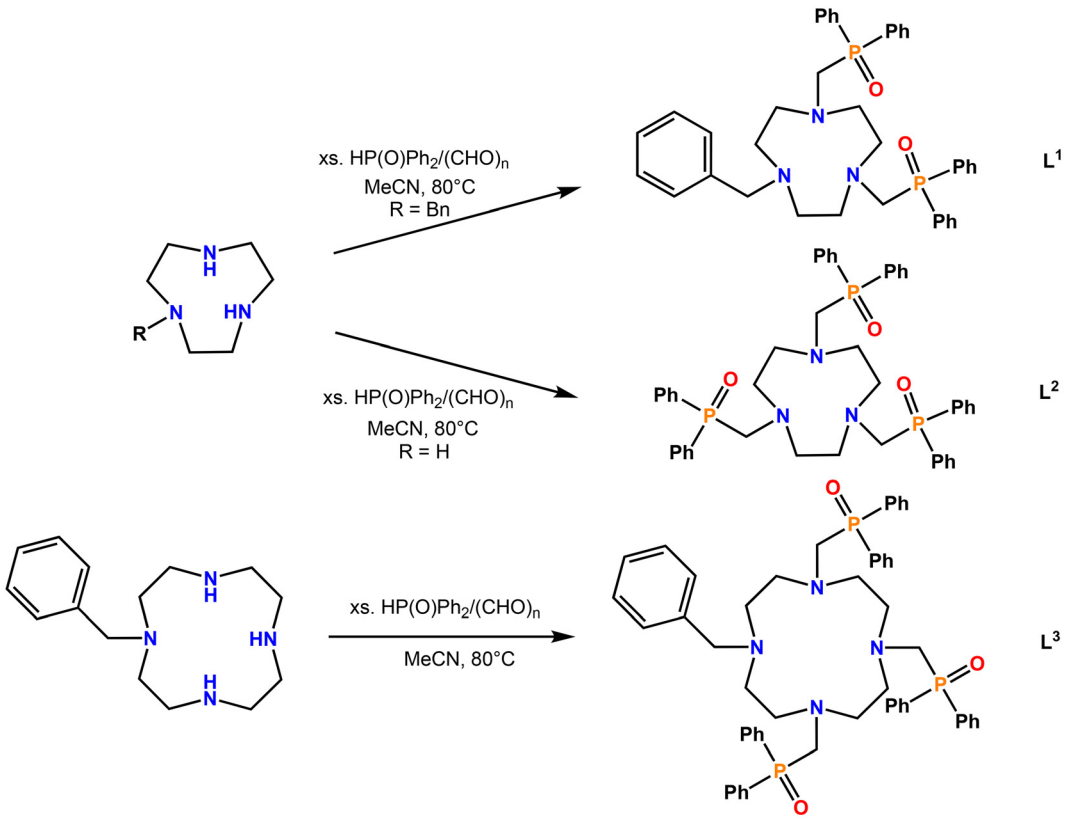

Scheme 2 Synthesis routes used to prepare L^1–L^3.

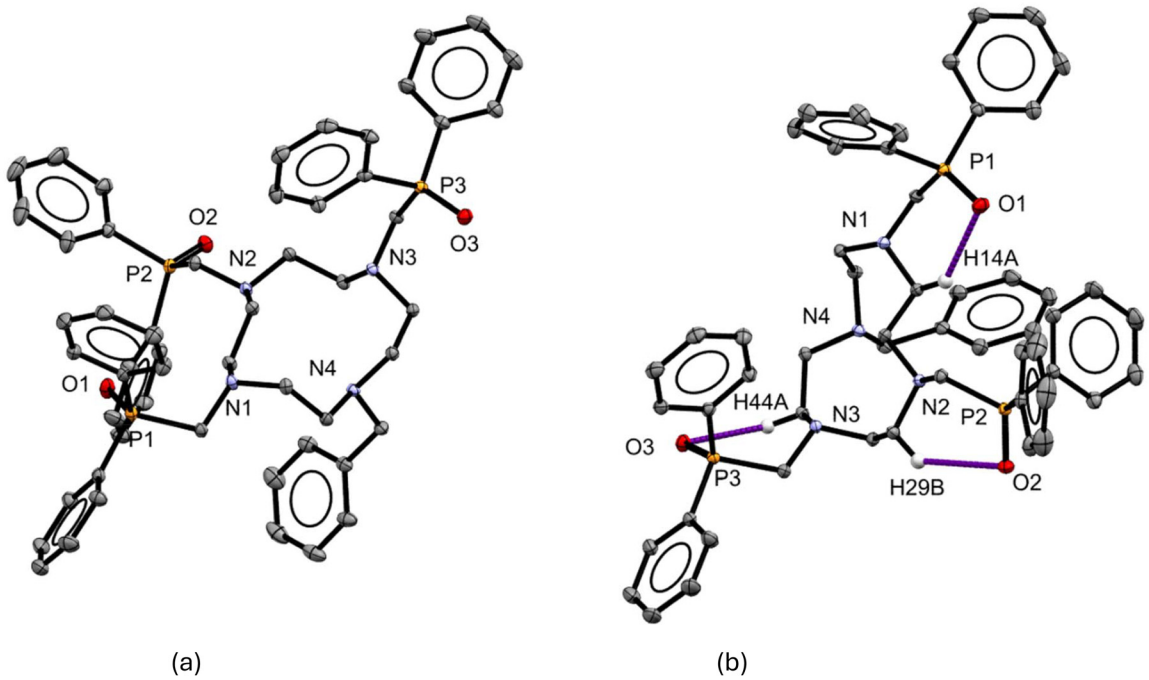

Fig. 1 (a) Structure of L^3·MeCN with the H-atoms (except those involved in the O···H contacts) and lattice solvent omitted for clarity. Ellipsoids are drawn at the 50% probability level; (b) figure showing the close contacts between the phosphoryl oxygen atoms each with a C–H on the cyclen ring. Selected bond lengths (Å): P1–O1 = 1.4935(10), P2–O2 = 1.4910(9), P3–O3 = 1.4921(9), O1···H14A = 2.4007(10), O2···H29B = 2.5117(9), O3···H44A = 2.4495(9).

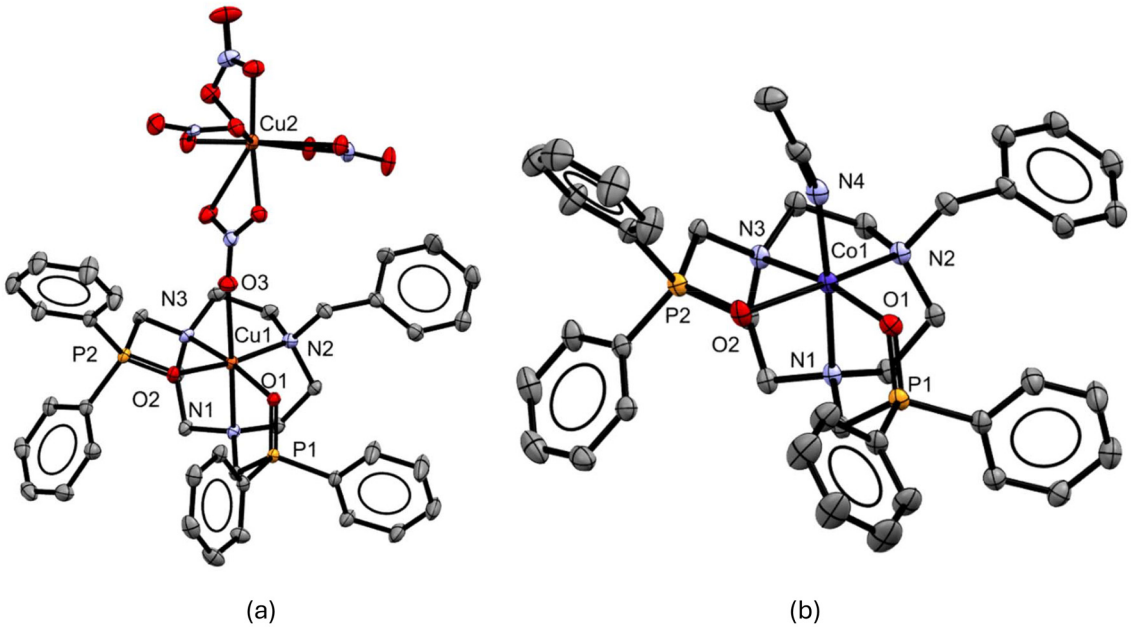

Fig. 2 (a) Structure of $[Cu(L^1)\{Cu(NO_3)_4\}]$ with the H-atoms omitted for clarity. Ellipsoids are drawn at the 50% probability level; (b) structure of the cation in $[Co(L^1)(MeCN)][BPh_4]_2{\cdot}MeCN$ with the H-atoms, anions and lattice MeCN omitted for clarity. Ellipsoids are drawn at the 50% probability level.

shown in Fig. 2(b), while views of the structures with the other metal ions are shown in the SI, Fig. S16(a) and (b). Key bond lengths for these $\mathbf{L^1}$ complexes are presented in Table 1. The three complexes are isostructural, with $\mathbf{L^1}$ coordinating in a pentadentate manner, and the sixth coordination site occupied by the acetonitrile ligand, in accord with the spectroscopic and analytical data. The cations have an approximate octahedral geometry with twist angles ranging from 54.17(4)–57.15(4)° (twist angle of an octahedron = 60°).

Similarly, reaction of $\mathbf{L^2}$ with 2 mol. equiv. of $Cu(NO_3)_2{\cdot}3H_2O$ in MeOH solution yielded $[Cu(\mathbf{L^2})][Cu(NO_3)_4]$, while the $[M(\mathbf{L^2})][BPh_4]_2$ salts were readily isolated from a 1 : 1 $M : \mathbf{L^2}$ ratio, followed by precipitation of the $[BPh_4]^-$ salts for M = Co, Ni, Zn. Spectroscopic analysis and microanalyses for these products are all consistent with hexadentate coordination of $\mathbf{L^2}$ *via* its N_3O_3 donor set.

Single crystals suitable for X-ray diffraction were also obtained for all four complexes as described in the Experimental section. In each case the structures confirm six-coordinate metal cations *via* the N_3O_3 macrocyclic donor set (Fig. 3(a) and (b), Table 2 and Fig. S17); the Co, Ni and Zn complexes are isostructural. The twist angles (Table 2) indicate a distorted octahedral geometry in each case. The average M–N distances follow the trend expected from the ionic radii of the divalent cations (Fig. 4), while the M–O distances all fall within a similar range, except with copper. For $[Cu(\mathbf{L^2})][Cu(NO_3)_4]$ the Jahn–Teller effect causes a compression of the Cu1–O1 and Cu1–N3 bonds, contrasting with the tetragonally elongated $[Cu(\mathbf{L^1})\{Cu(NO_3)_4\}]$. In all cases the metal sits closer to the plane defined by the three O atoms than that of the N donor atoms.

Similarly to ligand $\mathbf{L^2}$, complexes of $\mathbf{L^3}$ with the late divalent transition metals were isolated (*vide supra*), either as $[Cu(\mathbf{L^3})][Cu(NO_3)_4]$, or, for the rest as their $[BPh_4]^-$ salts, $[M(\mathbf{L^3})][BPh_4]_2$, M = Co, Ni, Zn. Despite significant effort we were unable to obtain crystals of $[M(\mathbf{L^3})][BPh_4]_2$ suitable for X-ray diffraction studies, however, for M = Zn, Co, and Ni crystals of the nitrate salts $[M(\mathbf{L^3})][NO_3]_2$ were obtained from a small aliquot of the solutions prior to addition of $Na[BPh_4]$. The crystal structures show (Fig. 6) that all four N-donor atoms from the cyclen ring are bound to the metal centre, as well as the two phosphine oxide pendant groups on the N atoms adjacent to the benzyl group, leaving the third phosphine oxide group uncoordinated. This gives rise to an N_4O_2 donor set at

Table 1 Key bond lengths for the complexes $[M(L^1)(MeCN)][BPh_4]_2$ (M = Ni, Zn, Co) and $[Cu(L^1)\{Cu(NO_3)_4\}]$

Bond	M = Co/Å	M = Ni/Å	M = Cu/Å	M = Zn/Å
M–O1	2.0472(13)	2.0567(12)	1.9745(9)	2.0441(12)
M–O2	2.1126(13)	2.0981(12)	1.9823(9)	2.1187(13)
M–N1(tacn)	2.1724(16)	2.1002(14)	2.2548(12)	2.2053(15)
M–N2(tacn)	2.1552(14)	2.0567(12)	2.0395(11)	2.1749(15)
M–N3(tacn)	2.1722(15)	2.0997(14)	2.0348(11)	2.2074(15)
M–N4(MeCN)	2.1118(18)	2.0765(16)	–	2.1441(18)
P1–O1	1.5169(14)	1.5105(12)	1.5194(10)	1.5140(13)
P2–O2	1.5105(14)	1.5128(13)	1.5167(10)	1.5089(13)
Twist angle/° [a]	55.59(4)	57.15(4)	54.87(3)	54.17(4)

[a] Defined as the angle, α, between the triangular face defined by the tacn N atoms and the face defined by the coordinating oxygens of the arms and the coordinated MeCN or Cu anion.

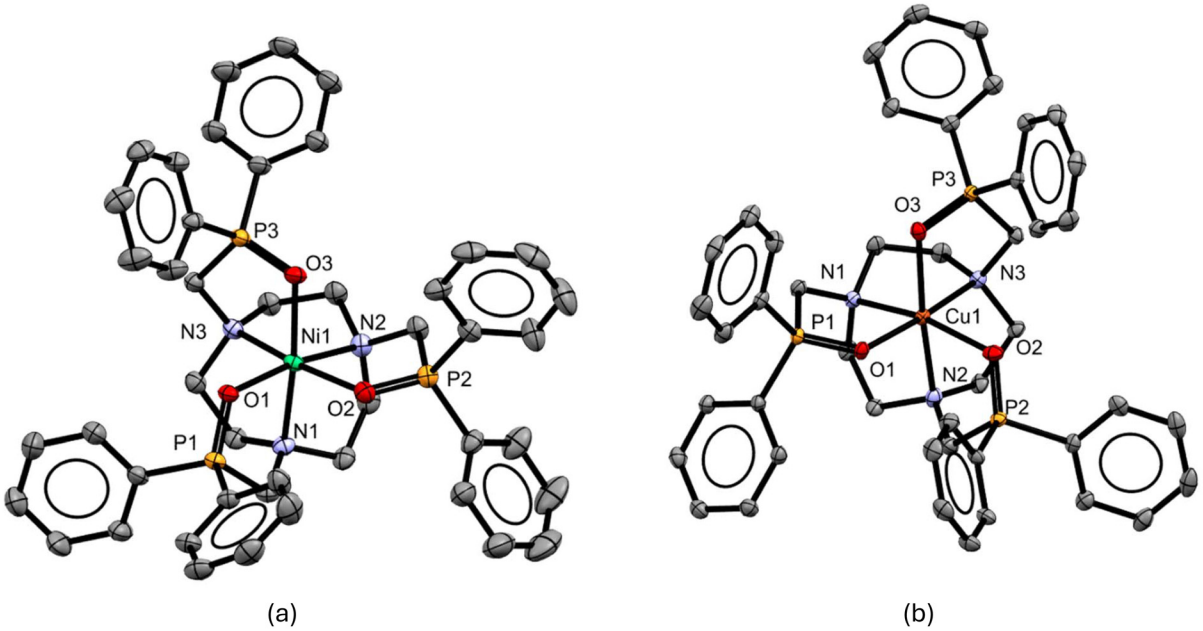

Fig. 3 Crystal structures of the cations in (a) $[Ni(L^2)][BPh_4]_2$ and (b) $[Cu(L^2)][Cu(NO_3)_4]$ with H atoms and counter anions omitted for clarity. Ellipsoids are drawn at the 50% probability level.

Table 2 Selected cation bond lengths and twist angles for the complexes $[M(L^2)][BPh_4]_2$ (M = Ni, Zn, Co) and $[Cu(L^2)][Cu(NO_3)_4]$

Bond	M = Co/Å	M = Ni/Å	M = Cu/Å	M = Zn/Å
M–O1	2.0783(11)	2.0551(13)	1.9613(19)	2.0554(11)
M–O2	2.0669(10)	2.0885(15)	2.127(2)	2.0445(11)
M–O3	2.1034(11)	2.0675(14)	2.1333(19)	2.0806(12)
M–N1	2.1584(12)	2.0989(16)	2.166(2)	2.2018(14)
M–N2	2.1697(13)	2.0990(17)	2.212(2)	2.2212(13)
M–N3	2.1582(13)	2.0854(18)	2.032(2)	2.2032(14)
P1–O1	1.5100(11)	1.5068(14)	1.5196(19)	1.5136(12)
P2–O2	1.5108(11)	1.5079(15)	1.509(2)	1.5124(11)
P3–O3	1.5081(11)	1.5058(15)	1.5114(19)	1.5100(12)
Twist angle/° [a]	50.24(3)	52.29(4)	52.41(6)	49.63(3)

[a] Defined as the angle, α, between the triangular face defined by the tacn N atoms and the face defined by the coordinating oxygens of the arms.

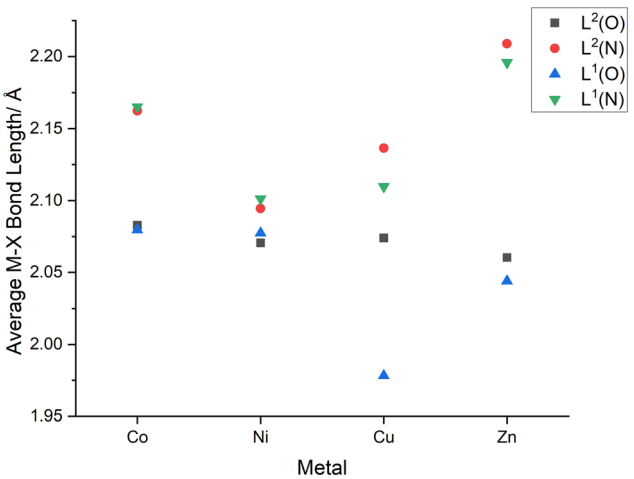

Fig. 4 Graph illustrating how the average M–X bond lengths (X = O, N) change with the metal in the L^1 and L^2 complexes.

each metal ion, with the O-donor atoms mutually *cis*, the small ring-size of the cyclen prevents *trans* coordination of the pendant arms. For the cobalt and zinc complexes the geometries around the metal are approximately trigonal prismatic (twist angles of 11.35(10)° and 11.13(7)°, respectively), contrasting with the complexes with L^1 and L^2 discussed above and also contrasting with $[M(\textbf{DOTP-Ph})]^{2+}$ (M = Co, Zn) which have eight-coordinate twisted square antiprismatic geometries (Table 3).[13]

For $[Ni(L^3)][NO_3]_2$, although the diffraction data quality was poor, it does indicate that the cation geometry is approximately octahedral (twist angle = 59.73(18)°), contrasting with the zinc and cobalt complexes, although as in the zinc and cobalt complexes, it is the phosphine oxide opposite the benzyl group that remains uncoordinated and the nitrates are not involved in the metal coordination sphere. The $^{31}P\{^1H\}$ and ^1H NMR spectra of the zinc complex are in accord with the geometry observed in the solid state; the $^{31}P\{^1H\}$ NMR spectrum shows two resonances at 34.0 and 24.4 ppm in a 2 : 1 ratio consistent with the two phosphine oxides on the N atoms closest to the benzyl group coordinating to the metal centre in a symmetrical manner, with the other remaining uncoordinated. In the ^1H NMR spectrum of $[Zn(L^3)][BPh_4]_2$ (Fig. 5) there is a pair of resonances at 3.93 ppm corresponding to the pair of diastereotopic protons on the methylene bridge of the coordinated phosphine oxide arms, consistent with retention of the solid-state structure in solution. The protons were

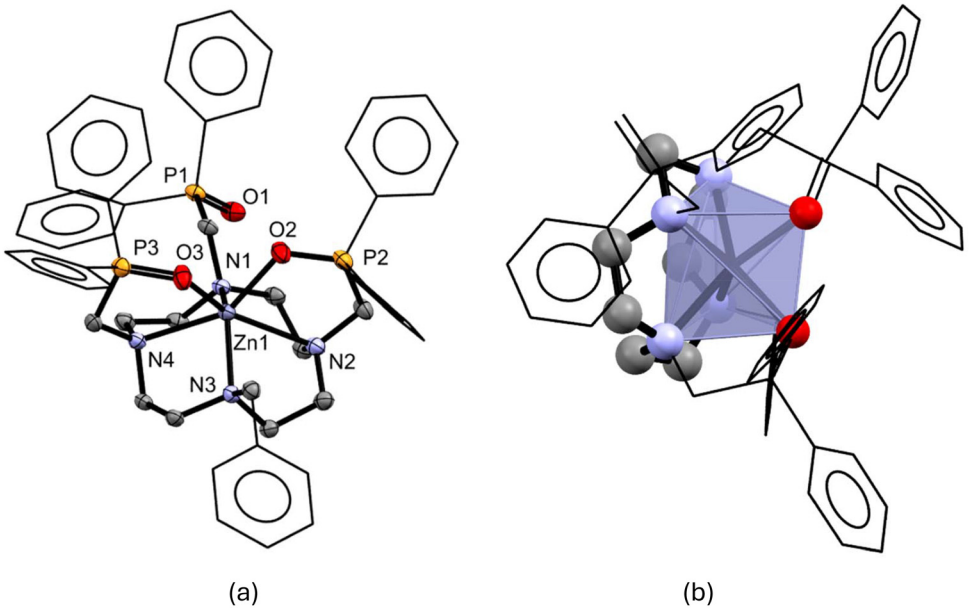

Fig. 6 (a) Structure of cation in $[Zn(L^3)][NO_3]_2$ with the H-atoms, counter anions and lattice solvent omitted for clarity and Ph rings are shown as wire-frame. Ellipsoids are drawn at the 50% probability level. Selected bond lengths (Å) and angles (°): Zn1–N1 = 2.190(3), Zn1–N2 = 2.486(2), Zn1–N3 = 2.1238(2), Zn1–N4 = 2.349(3), Zn1–O2 = 2.032(2), Zn1–O3 = 2.102(2), P1–O1 = 1.487(2), P2–O2 = 1.513(3), 1.509(2), N2–Zn1–O3 = 149.04(9), N4–Zn1–O2 = 150.51(9), N1–Zn1–N3 = 128.33(9), O2–Zn1–O3 = 80.41(9); mean twist angle = 11.13(7)°; (b) a polyhedral model of $[Zn(L^3)]^{2+}$ showing the trigonal prismatic coordination geometry.

Table 3 Summary of the coordination numbers and geometries of the divalent complexes formed with L^1–L^3

	L^1	L^2	L^3	DOTP-Ph [13]
Co	6 (oct.)	6 (oct.)	6 (trig. prism)	8 (twisted sq. antiprism)
Ni	6 (oct.)	6 (oct.)	6 (oct.)	6 (oct.)
Cu	6 (J–T elongated oct.)	6 (J–T compressed oct.)	—	5 (dist. tetragonal pyr.)
Zn	6 (oct.)	6 (oct.)	6 (trig. prism)	8 (twisted sq. antiprism)

shown to be in the same spin system by cross peaks in the ^1H–^1H COSY NMR spectrum (SI, Fig. S15.3).

For the tacn-based ligands L^1 and L^2 the overall geometries of the complexes are independent of the metal, except for copper(II) where Jahn–Teller distortions are seen in both cases. The manifestation of the Jahn–Teller effect is ligand dependent, with L^1 giving a tetragonal elongation and L^2 giving tetragonal compression. For the cyclen-based ligands L^3 and **DOTP-Ph** the geometries depend both on the ligand and the metal. With L^3 both cobalt and zinc form trigonal prismatic cations, while the nickel(II) ion appears to adopt a coordination environment closer to octahedral. This contrasts with the previously reported complexes with **DOTP-Ph** where the coordination environment depends strongly on the metal, with copper(II) forming a five-coordinate complex *via* the four cyclen nitrogens and one phosphine oxide arm, and both cobalt(II) and zinc(II) forming unusual eight-coordinate complexes with the **DOTP-Ph** octadentate.[12]

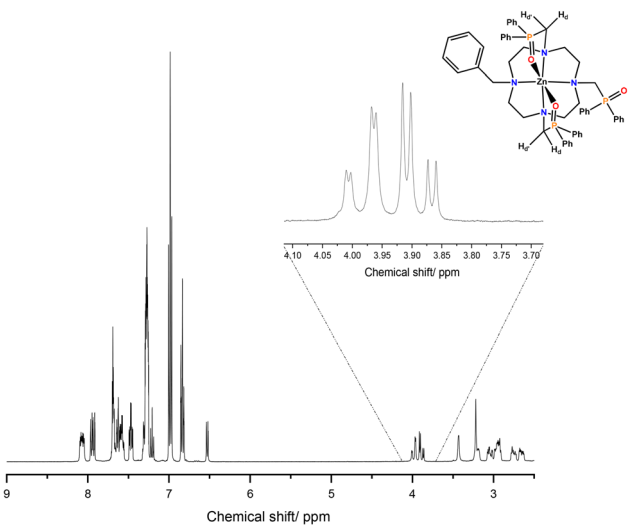

Fig. 5 ^1H NMR spectrum of $[Zn(L^3)][BPh_4]_2$ in CD_3CN. The expansion (top right) shows the resonance from the diastereotopic methylene protons from the coordinated phosphine oxide arms.

Experimental

Metal salts, reagents and solvents (Fisher and Sigma-Aldrich) were used as received, while the macrocycles, Bn-tacn, tacn, and Bn-cyclen, were sourced from Chematech. Ligand preparations were undertaken under a dry N_2 atmosphere using Schlenk techniques.

Infrared spectra were recorded using a Thermo Scientific Nicolet iS5 ATIR spectrometer (4000–400 cm^{-1}). ^{1}H, $^{13}C\{^{1}H\}$ and $^{31}P\{^{1}H\}$ NMR spectra were recorded using a Bruker AV400 or AVIIIHD400 spectrometer. Spectra were referenced to $SiMe_4$ (TMS) *via* the residual solvent resonance (^{1}H and $^{13}C\{^{1}H\}$) and external 85% H_3PO_4 ($^{31}P\{^{1}H\}$). Low resolution ESI^+ mass spectra for the metal complexes were acquired using a Waters (Manchester, UK) Acquity UPC2 TQD tandem quadrupole mass spectrometer. Samples were introduced using a 2 μL Partial Loop with Needle Overfill (PLNO) injection. High resolution ESI^+ mass spectra were obtained using a Waters (Manchester, UK) Acquity TQD mass tandem quadrupole mass spectrometer. Samples were introduced to the mass spectrometer *via* an Acquity H-Class quaternary solvent manager (with TUV detector at 254 nm, sample and column manager). Ultrahigh performance liquid chromatography was undertaken using Waters BEH C18 column (50 mm × 2.1 mm 1.7 μm). Gradient elution from 20% acetonitrile (0.2% formic acid) to 100% acetonitrile (0.2% formic acid) was performed over five/ten minutes at a flow rate of 0.6 mL min^{-1}. A Johnson Matthey magnetic balance was used to take magnetic measurements. Diamagnetic corrections were used for Co(II) and Ni(II) as -12×10^{-6} emu mol^{-1}, whilst the approximation of $X_{dia} = -(MW/2) \times 10^{-6}$ emu mol^{-1} was used for the ligands and anions present. UV/vis data were obtained using a PerkinElmer Lambda 750 S Spectrometer using acetonitrile as the solvent across a range of 1300–300 nm. Duplicate microanalyses were carried out at Medac Ltd.

X-ray crystallography

Data collections used a Rigaku UG2 goniometer equipped with a Rigaku HyPix-6000HE hybrid pixel detector mounted at the window of an FR-E+ SuperBright molybdenum (λ = 0.71073 Å) rotating anode generator with HF Varimax optics (100 μm focus) with the crystal held at 100 K, or a Rigaku UG2 goniometer equipped with a Rigaku Hypix 6000 HE detector mounted at the window of an FR-E+ SuperBright molybdenum (λ = 0.71073 Å) rotating anode generator with ArcSec VHF Varimax confocal mirrors (70 μm focus), with the crystal held at 100 K. Structure solution and refinement were performed using SHELXT-2018/2[16] and SHELXL-2018/3[17] *via* Olex2.[18] The solution and refinement of the complexes was mostly routine, although for the complex $[Ni(\mathbf{L^1})(MeCN)][BPh_4]_2$·MeCN there was disorder in the lattice MeCN and one of the ligand phenyl rings, which was modelled using split occupancies (50 : 50 split in each case). For $[Co(\mathbf{L^3})][NO_3]_2$ there was electron density (320 electrons in cell) that could not be satisfactorily modelled, so a solvent mask was applied, which corresponds to 2 Et_2O per asymmetric unit. In this structure one of the phenyl groups was also disordered over two sites with a ratio of 0.74 : 0.26 and modelled satisfactorily by split occupancies. For $[Zn(\mathbf{L^3})][NO_3]_2$ there was also residual electron density (546 electrons in the cell) for which a solvent mask was applied, corresponding to 6 MeCN molecules per asymmetric unit. The crystallographic parameters are given in SI Table S16. The diffraction from $[Ni(\mathbf{L^3})][NO_3]_2$ gave broad diffuse reflections observed at low angle only and data higher than 1.0 Å resolution had an $I/\sigma < 3$. Whilst it was possible to refine a chemically sensible structure and connectivity, it was not possible to obtain refinement statistics that meet the generally acceptable criteria for publication or inclusion in the Cambridge Crystallographic Database.

Ligand syntheses

$\mathbf{L^1}$. Bn-tacn (0.750 g, 3.42 mmol) was dissolved in 6 mL of dry MeCN, to this paraformaldehyde (0.256 g, 8.52 mmol), was added and then diphenylphosphine oxide (1.727 g, 8.54 mmol), to form a cloudy solution. This was heated to 80 °C for 10 min, giving a clear orange solution. Heating was continued for 2 h until the starting materials had been consumed (by ESI^+ MS). The solvent was removed *in vacuo*, and the crude product was purified by column chromatography on neutral alumina by elution with 0–2% MeOH : CH_2Cl_2, with the target compound eluted first. Fractions containing $\mathbf{L^1}$ were combined, dried over Na_2SO_4 and the solvent removed *in vacuo* to give an off-white powder. Yield: 0.969 g (44%). ^{1}H NMR (298 K, CD_3CN): δ (ppm) = 7.78–7.73 (m, [8H], Ar*H*), 7.53–7.45 (m, [12H], Ar*H*), 7.35–7.13 (m, [5H], Ar–*H*), 3.62 (br s, [2H], CH_2Ph), 3.36 (d, $^{2}J_{HP}$ = 4.3 Hz, [4H], CH_2P), 2.81 (br m, [4H], tacn-CH_2), 2.60–2.32 (br m, [8H], tacn-CH_2). $^{13}C\{^{1}H\}$ NMR (298 K, CD_3CN): δ (ppm) = 133.5 (d, $^{1}J_{PC}$ = 93.9 Hz, *ipso-C*, PPh), 132.3 (s, *p-C*H, PPh), 131.5 (d, $^{3}J_{PC}$ = 8.8 Hz, *m-C*H, PPh), 130.2 (s, *p-C*H, Bn), 129.2 (d, $^{2}J_{PC}$ = 11.0 Hz, *o-C*H, PPh), 128.9 (s, *o-C*H, Bn), 61.9 (s, NCH_2Bn), 58.1 (d, $^{1}J_{PC}$ = 84.4 Hz, NCH_2P), 56.9 (br d, 2 × tacn-CH_2), 54.2 (s, tacn-CH_2NBn); *ipso-C* of Bn and *m-C*H, Bn not observed. $^{31}P\{^{1}H\}$ NMR (298 K, CD_3CN): δ (ppm) = 27.8 (s). IR (ATIR, ν/cm^{-1}): 1179 (P═O). HR ESI^+ MS (MeOH); found: m/z = 648.2906 $[C_{39}H_{43}N_3O_2P_2 + H]^+$ (calculated for $[C_{39}H_{43}N_3O_2P_2 + H]^+$ = 648.2903).

$\mathbf{L^2}$. Tacn (0.500 g, 3.87 mmol) and diphenylphosphine oxide (2.35 g, 11.6 mmol) were dissolved in dry MeCN (5 ml), resulting in a cloudy solution, paraformaldehyde (0.348 g, 11.6 mmol) was then added to give a cloudy pale-yellow solution. This was heated to 80 °C and stirred for 3 h, during which time the solution became a clear yellow colour. The crude product was isolated by removing the solvent *in vacuo* to leave a yellow powder which was purified using column chromatography on alumina by eluting with 0–2% MeOH : CH_2Cl_2. Fractions containing $\mathbf{L^2}$ were combined and dried *in vacuo*, affording an off-white powder. Yield: 0.725 g (24%). ^{1}H NMR (CD_3CN, 298 K): δ (ppm) = 7.75–7.46 (br, [30H], Ar*H*), 3.32 (d, $^{2}J_{HP}$ = 4.78 Hz, [6H], NCH_2P), 2.57 (s, [12H], tacn-CH_2). $^{13}C\{^{1}H\}$ NMR (298 K, $CDCl_3$): δ (ppm) = 132.4 (d, $^{1}J_{PC}$ = 96.1 Hz, *ipso-C*, PPh), 131.8 (s, *p-C*H, PPh), 131.2 (d, $^{3}J_{PC}$ = 8.8 Hz, *m-C*H, PPh), 128.6 (d, $^{2}J_{PC}$ = 11.0 Hz, *o-C*H, PPh), 58.3 (d, $^{1}J_{PC}$ = 85.8 Hz, NCH_2P), 56.7 (s, tacn-CH_2). $^{31}P\{^{1}H\}$ NMR (CD_3CN): δ (ppm) = 26.0 (s, P═O). IR (ν/cm^{-1}): 1174 (P═O). HR ESI^+ MS (MeOH); found: m/z = 772.2945 $[C_{45}H_{48}N_3O_3P_3 + H]^+$, 794.2763 $[C_{45}H_{48}N_3O_3P_3 + Na]^+$ (calculated for $[C_{45}H_{48}N_3O_3P_3 + H]^+$ = 772.2981, $[C_{45}H_{48}N_3O_3P_3 + Na]^+$ 794.2801).

$\mathbf{L^3}$. Bn-cyclen (0.750 g, 2.85 mmol) was dissolved in dry MeCN (5 ml) to form a clear colourless solution.

Paraformaldehyde (0.772 g, 25.7 mmol) was added, followed by diphenylphosphine oxide (5.202 g, 25.7 mmol) was added and the mixture was heated to 80 °C. After 15 min the solution was a clear yellow, and after 22 h the starting material was consumed (according to ESI^+). The crude product was isolated by removing the solvent *in vacuo*, and purified by column chromatography with neutral alumina, 0–1% MeOH in CH_2Cl_2. Fractions containing $\mathbf{L^3}$ were combined and dried over $MgSO_4$ and the solvent removed *in vacuo* to yield the ligand as an off-white powder. Yield: 1.115 g (43%). ^1H NMR (298 K, CD_3CN): δ (ppm) = 7.80–7.70 (m, [12H], Ar–*H*), 7.53–7.43 (m, [18H], Ar–*H*), 7.29–7.16 (m, [5H], Ar–*H*), 3.31 (br s, [2H], CH_2Ph), 3.30 (d, $^2J_{PH}$ = 4.5 Hz, [2H], CH_2PPh$_2$), 3.23 (d, $^2J_{PH}$ = 4.2 Hz, [4H], CH_2PPh$_2$), 2.65–2.61 (m, [12H], cyclen-*H*), 2.23 (br s, [4H], cyclen-*H*). $^{13}C\{^1H\}$ NMR (298 K, CD_3CN): δ (ppm) = 133.8 (d, $^1J_{PC}$ = 95.4 Hz, *ipso-C*, PPh), 132.6 (s, *p-C*H, unique PPh), 132.4 (s, *p-C*H, PPh), 131.8 (d, $^3J_{PC}$ = 9.5 Hz, *m-C*H, unique PPh), 131.5 (d, $^3J_{PC}$ = 8.1 Hz, *m-C*H, PPh), 130.8 (s, *p-C*H, Bn), 129.3 (d, $^2J_{PC}$ = 11.0 Hz, *o-C*H, unique PPh), 129.2 (d, $^2J_{PC}$ = 11.0 Hz, *o-C*H, PPh), 128.9 (s, *o-C*H, Bn), 59.3 (*C*H$_2$ of Bn), 55.5 (d, $^1J_{PC}$ = 87.0 Hz, *C*H$_2$P), 54.5 (br, overlapping cyclen *C*H$_2$), 53.0, 51.8 (cyclen *C*H$_2$). $^{31}P\{^1H\}$ NMR (CD_3CN): δ (ppm) = 27.4 (s, [2P]), 27.3 (s, [1P]). IR (ATIR, ν/cm^{-1}): 1175 (P═O). HR ESI^+ MS (MeOH); found: *m*/*z* = 905.3863 $[C_{54}H_{59}N_4O_3P_3 + H]^+$, 927.3691 $[C_{54}H_{59}N_4O_3P_3 + Na]^+$, 453.1974 $[C_{54}H_{59}N_4O_3P_3 + 2H]^{2+}$ (calculated for $[C_{54}H_{59}N_4O_3P_3 + H]^+$ = 905.3873, $[C_{54}H_{59}N_4O_3P_3 + Na]^+$ = 927.3692, $[C_{54}H_{59}N_4O_3P_3 + 2H]^{2+}$ = 453.1973).

Metal complexes

$[Co(\mathbf{L^1})(MeCN)][BPh_4]_2$. To a solution of $Co(NO_3)_2{\cdot}6H_2O$ (0.034 g, 0.117 mmol) in MeOH (2 mL) was added $\mathbf{L^1}$ (0.075 g, 0.116 mmol) in MeOH (1 mL), giving a deep pink coloured solution which was stirred for 1 h. $Na[BPh_4]$ (0.079 g, 0.231 mmol) dissolved in MeOH (2 mL) was then added, causing precipitation of a pink solid which was isolated by filtration and dried *in vacuo*. Yield: 0.102 g (65%). Required for $C_{89}H_{86}B_2CoN_4O_2P_2{\cdot}MeCN$ (1427.21): C, 76.58; H, 6.29; N, 4.91. Found: C, 75.93; H, 6.23; N, 4.48%. UV-vis (MeCN), 3×10^{-3} M: λ_{max}/nm (ε/M^{-1} cm^{-1}): 474 (39), 513 (27), 1097 (12). IR spectrum (powder, ν/cm^{-1}): 1136 (P═O), 2269, 2296 (MeCN). ESI^+ MS (MeCN): (calculated for $[Co(\mathbf{L^1})]^{2+}$: 353.11); found: *m*/*z* = 353.23 $[Co(\mathbf{L^1})]^{2+}$. Single crystals were grown *via* slow evaporation of MeCN from a solution of the complex.

$[Ni(\mathbf{L^1})(MeCN)][BPh_4]_2$. Method as above, using $Ni(NO_3)_2{\cdot}6H_2O$ (0.034 g, 0.117 mmol), $\mathbf{L^1}$ (0.075 g, 0.116 mmol) and $Na[BPh_4]$ (0.079 g, 0.0231 mmol). Light green powder. Yield: 0.074 g (47%). Required for $C_{89}H_{86}B_2N_4NiO_2P_2{\cdot}MeCN{\cdot}2H_2O$ (1463.00): C, 74.71; H, 6.41; N, 4.79. Found: C, 74.16; H, 6.05; N, 4.37%. UV-vis (MeCN), 3×10^{-3} M: λ_{max}/nm (ε/M^{-1} cm^{-1}): 368 (40), 577 (11), 992 (18). IR spectrum (powder, ν/cm^{-1}): 1137 (P═O), 2271, 2300 (MeCN). ESI^+ MS (MeCN): (calculated for $[Ni(\mathbf{L^1})]^{2+}$: 352.61); found: *m*/*z* = 352.79 $[Ni(\mathbf{L^1})]^{2+}$. Single crystals were grown *via* slow evaporation of MeCN from a solution of the complex.

$[Zn(\mathbf{L^1})(MeCN)][BPh_4]_2$. Method as above, using $Zn(NO_3)_2{\cdot}6H_2O$ (0.034 g, 0.114 mmol), $\mathbf{L^1}$ (0.075 g, 0.116 mmol) and $Na[BPh_4]$ (0.079 g, 0.231 mmol). White powder. Yield: 0.093 g, (60%). Required for $C_{89}H_{86}B_2N_4O_2P_2Zn{\cdot}MeCN$ (1433.67): C, 76.24; H, 6.26; N, 4.88. Found: C, 75.66; H, 6.23; N, 4.48%. ESI^+ MS (MeCN): (calculated for $[Zn(\mathbf{L^1})]^{2+}$: 355.61); found: *m*/*z* = 355.69 $[Zn(\mathbf{L^1})]^{2+}$. ^1H NMR (CD_3CN): δ (ppm) = 7.96–7.61 (m, [20H], $\mathbf{L^1}$ Ar–*H*), 7.35 (m, [3H], $\mathbf{L^1}$ Ar–*H*), 7.25 (m, [16H], BPh_4), 7.18 (m, [2H], $\mathbf{L^1}$ Ar–*H*), 6.96 (m, [16H], BPh_4), 6.78 (m, [8H], BPh_4), 4.01 (s, [2H], NCH_2Ph), 3.97 (d, $^2J_{PH}$ = 4 Hz, [4H], NCH_2PPh$_2$), 2.91–2.71 (m, [8H], tacn-CH_2), 2.48 (m, [2H], tacn-CH_2), 2.18 (m, [2H], tacn-CH_2); the 3H atoms associated with the coordinated MeCN are masked by the residual protio signal from the CD_3CN solvent. $^{31}P\{^1H\}$ NMR (CD_3CN): δ (ppm) = 35.9 (s). IR (powder, ν/cm^{-1}): 1136 (P═O), 2269, 2297 (MeCN).

$[Cu(\mathbf{L^1})\{Cu(NO_3)_4\}]$. $Cu(NO_3)_2{\cdot}3H_2O$ (0.056 g, 0.232 mmol) was dissolved in MeOH (1 mL) and a solution of $\mathbf{L^1}$ (0.075 g, 0.116 mmol) in MeOH (1 mL) was added, giving a green solution. This was stirred for 1 h, after which 5 mL of Et_2O was added to cause precipitation of a blue-green powder which was isolated by filtration and dried *in vacuo*. Yield: 0.042 g, (35%). Required for $C_{39}H_{43}Cu_2N_7O_{14}P_2{\cdot}Et_2O$ (1096.90): C, 47.1; H, 4.9; N, 8.9. Found: C, 47.2; H, 4.6; N, 9.1%. ESI^+ MS (MeCN): (calculated for $[Cu(\mathbf{L^1})]^{2+}$: *m*/*z* = 355.1058); found: *m*/*z* = 355.1052 $[Cu(\mathbf{L^1})]^{2+}$. IR (ATIR, ν/cm^{-1}): 1123 (P═O). UV-vis (MeCN, 3×10^{-3} M: λ_{max}/nm (ε/M^{-1} cm^{-1})): 757 (54).

$[Co(\mathbf{L^2})][BPh_4]_2$. $Co(NO_3)_2{\cdot}6H_2O$ (0.028 g, 0.097 mmol) was dissolved in MeOH (5 mL) under N_2 and $\mathbf{L^2}$ (0.075 g, 0.097 mmol) was added, resulting in a deep pink solution which was stirred for 1 h at room temperature. $NaBPh_4$ (0.100 g, 0.291 mmol) was then added, affording a light pink precipitate, which was isolated by filtration and dried *in vacuo* giving a pale pink powder. Yield: 0.096 g (67%). Required for $C_{93}H_{88}B_2CoN_3O_3P_3{\cdot}2H_2O$ (1505.22): C, 74.21; H, 6.16; N, 2.79. Found: C, 74.27; H, 6.15; N, 2.71%. ESI^+ MS (MeCN): (calculated for $[Co(\mathbf{L^2})]^{2+}$: *m*/*z* = 415.11); found: *m*/*z* = 415.18 $[Co(\mathbf{L^2})]^{2+}$. IR (ν/cm^{-1}): 1134 s (P═O). UV-vis (MeCN), 3×10^{-3} M: λ_{max}/nm (ε/M^{-1} cm^{-1}): 511 (51), 541 (47), 1200 (16). Crystals suitable for single crystal X-ray analysis were grown by vapour diffusion of Et_2O into an MeCN solution of the complex.

$[Ni(\mathbf{L^2})][BPh_4]_2$. Method as above, using $Ni(NO_3)_2{\cdot}6H_2O$ (0.028 g, 0.097 mmol), $\mathbf{L^2}$ (0.075 g, 0.097 mmol) and $NaBPh_4$ (0.099 g, 0.291 mmol). Green-blue solid. Yield: 0.092 g (64%). Required for $C_{93}H_{88}B_2NiN_3O_3P_3{\cdot}H_2O$ (1486.96): C, 75.12; H, 6.10; N, 2.83. Found: C, 75.25; H, 5.96; N, 2.89%. ESI^+ MS (MeCN): (calculated for $[Ni(\mathbf{L^2})]^{2+}$: *m*/*z* = 414.61); found: *m*/*z* = 414.98 $[Ni(\mathbf{L^2})]^{2+}$. IR (ν/cm^{-1}): 1134.90 s (P═O). UV-vis (MeCN, 3×10^{-3} M: λ_{max}/nm (ε/M^{-1} cm^{-1})): 376 (55), 604 (27), 1010 (30). Single crystals were grown *via* vapour diffusion of Et_2O into an MeCN solution of the complex.

$[Zn(\mathbf{L^2})][BPh_4]_2$. Method as above, using $Zn(NO_3)_2{\cdot}6H_2O$ (0.029 g, 0.097 mmol), $\mathbf{L^2}$ (0.075 g, 0.097 mmol) and $NaBPh_4$ (0.100 g, 0.291 mmol). White solid. Yield: 0.097 g (67%). Required for $C_{93}H_{88}B_2N_3O_3P_3Zn{\cdot}H_2O$ (1493.66): C, 74.78; H, 6.07; N, 2.81. Found: C, 74.34; H, 5.92; N, 2.90%. ^1H NMR (CD_3CN): δ (ppm) = 7.93–7.61 (*m*, [30H], Ar–*H*), 7.30–7.23 (*m*, [16H], BPh_4), 6.98 (*t*, $^2J_{HH}$ = 7.40 Hz, [16H], BPh_4), 6.83 (*t*, $^2J_{HH}$

= 7.22 Hz, [8H], BPh_4), 3.87 (*d*, $^2J_{HP}$ = 4.03 Hz, [6H], NCH_2P), 2.93–2.77 (*m*, [6H], tacn-CH_2), 2.67–2.52 (*m*, [6H], tacn-CH_2). $^{31}P\{^1H\}$ NMR (CD_3CN): δ (ppm) = 38.6 (s). ESI^+ MS (MeCN): (calculated for $[Zn(\mathbf{L^2})]^{2+}$: *m*/*z* = 417.61); found: *m*/*z* = 417.93 $[Zn(\mathbf{L^2})]^{2+}$. IR (ν/cm^{-1}): 1133 s (P═O). Crystals were grown *via* vapour diffusion of Et_2O into an MeCN solution of the complex.

$[Cu(\mathbf{L^2})][Cu(NO_3)_4]$. To a solution of the $Cu(NO_3)_2{\cdot}3H_2O$ (0.047 g, 0.194 mmol) in MeOH (2 mL) was added $\mathbf{L^2}$ (0.075 g, 0.097 mmol). The solution was stirred for 2 h and Et_2O (15 mL) was added, producing a light blue precipitate, which was isolated by filtration and dried *in vacuo*. Yield: 0.050 g (45%). Required for $C_{45}H_{48}Cu_2N_7O_{15}P_3{\cdot}H_2O$ (1164.93): C, 46.40; H, 4.33; N, 8.42. Found: C, 46.52; H, 4.11; N, 8.38%. ESI^+ MS (MeCN): (calculated for $[Cu(\mathbf{L^2})]^{2+}$: *m*/*z* = 417.11); found: *m*/*z* = 417.49 $[Cu(\mathbf{L^2})]^{2+}$. IR (ν/cm^{-1}): 1121 s (P═O). UV-vis (MeCN), 2.3 × 10^{-3} M: λ_{max}/nm (ε/M^{-1} cm^{-1}): 802 (120). Crystals were grown by vapour diffusion of Et_2O into an MeCN solution of the complex.

$[Co(\mathbf{L^3})][BPh_4]_2$. $Co(NO_3)_2{\cdot}6H_2O$ (0.013 g, 0.044 mmol) was dissolved in MeOH (2.5 mL) under nitrogen and $\mathbf{L^3}$ (0.040 g, 0.044 mmol) was added, giving a pink solution which was stirred for 40 min. $NaBPh_4$ (0.045 g, 0.132 mmol) was then added, producing a pink precipitate which was stirred for 1 h. The precipitate was separated by filtration and dried *in vacuo* leaving a pale pink solid. Yield: 0.044 g (62%). Required for $C_{102}H_{99}B_2CoN_4O_3P_3{\cdot}3H_2O$ (1656.42): C, 73.96; H, 6.39; N, 3.38. Found: C, 73.77; H, 6.01; N, 3.69%. ESI^+ MS (MeCN): (calculated for $[Co(\mathbf{L^3})]^{2+}$: *m*/*z* = 481.65); found: *m*/*z* = 481.56 $[Co(\mathbf{L^3})]^{2+}$. IR (ν/cm^{-1}): 1177 s (uncoordinated P═O), 1134 s (coordinated P═O). UV-vis (MeCN), 3 × 10^{-3} M: λ_{max}/nm (ε/M^{-1} cm^{-1}): 490 (64), 529 (50), 563 (48). Magnetic moment μ_{eff} = 4.92 B.M.

$[Ni(\mathbf{L^3})][BPh_4]_2$. Method as for the Co(II) analogue above, using $Ni(NO_3)_2{\cdot}6H_2O$ (0.013 g, 0.044 mmol), $\mathbf{L^3}$ (0.040 g, 0.044 mmol) and $NaBPh_4$ (0.045 g, 0.132 mmol). Light green powder. Yield: 0.045 g (64%). Required for $C_{102}H_{99}B_2NiN_4O_3P_3{\cdot}3H_2O$ (1656.18): C, 73.97; H, 6.39; N, 3.38. Found: C, 73.43; H, 6.14; N, 3.66%. ESI^+ MS (MeCN): (calculated for $[Ni(\mathbf{L^3})]^{2+}$: *m*/*z* = 481.16); found: *m*/*z* = 481.36 $[Ni(\mathbf{L^3})]^{2+}$. IR (ν/cm^{-1}): 1177 s (uncoordinated P═O), 1139 s (coordinated P═O). UV-vis (MeCN), 1.7 × 10^{-3} M: λ_{max}/nm (ε/M^{-1} cm^{-1}): 427 (52), 620 (27), 1138 (34)).

$[Zn(\mathbf{L^3})][BPh_4]_2$. Method as for the Co(II) analogue above using $Zn(NO_3)_2{\cdot}6H_2O$ (0.013 g, 0.044 mmol), $\mathbf{L^3}$ (0.040 g, 0.044 mol) and $NaBPh_4$ (0.030 g, 0.088 mmol). White solid. Yield: 0.040 g (57%). Required for $C_{102}H_{99}B_2N_4O_3P_3Zn{\cdot}3H_2O$ (1662.88): C, 73.67; H, 6.36; N, 3.37. Found: C, 73.67; H, 6.01; N, 3.57%. ^1H NMR (CD_3CN): δ (ppm) = 8.07 (m, [4H], lig-Ar*H*), 7.93 (m, [4H], lig-Ar*H*), 7.69–7.55 (m, [14H], lig-Ar*H*), 7.45 (m, [4H], lig-Ar*H*), 7.32–7.19 (m, [23H], Ar*H* + BPh_4), 6.99 (m, [16H], BPh_4), 6.84 (m, [8H], BPh_4), 6.53 (m, [2H], Ar*H*), 3.93 (m, [4H], coordinated –CH_2PO arms), 3.43 (d, $^2J_{HP}$ = 2.8 Hz, [2H], uncoordinated –CH_2PO arm), 3.22–3.18 (m, [4H], benzyl-CH_2 and cyclen-CH_2), 3.06–2.91 (m, [6H], cyclen-CH_2), 2.78–2.63 (m, [4H], cyclen-CH_2), 2.41 (m, [4H], cyclen-CH_2). $^{31}P\{^1H\}$ NMR (CD_3CN): δ (ppm) = 34.0 (s, [2P], coordinated P═O), 24.4 (s, [1P], uncoordinated P═O). ESI^+ MS (MeCN): (calculated for $[Zn(\mathbf{L^3})]^{2+}$: *m*/*z* = 484.15); found: *m*/*z* = 484.33 $[Zn(\mathbf{L^3})]^{2+}$. IR (ν/cm^{-1}): 1181 s (uncoordinated P═O), 1134 s (coordinated P═O).

$[Cu(\mathbf{L^3})][Cu(NO_3)_4]$. $Cu(NO_3)_2{\cdot}3H_2O$ (0.021 g, 0.088 mmol) was dissolved in MeOH (2 mL) under nitrogen and $\mathbf{L^3}$ (0.040 g, 0.044 mmol) was added to give a dark blue solution which was stirred for 30 min. Et_2O (10 mL) was then added, forming a blue precipitate which was isolated by filtration and dried *in vacuo*. Dark blue solid. Yield: 0.038 g (67%). Required for $C_{54}H_{59}Cu_2N_8O_{15}P_3{\cdot}2H_2O{\cdot}Et_2O$ (1372.24): C, 50.11; H, 5.29; N, 8.06. Found: C, 50.06; H, 4.98; N, 7.90%. ESI^+ MS (MeCN): (calculated for $[Cu(\mathbf{L^3})]^{2+}$: *m*/*z* = 483.65); found: *m*/*z* = 483.87 $[Cu(\mathbf{L^3})]^{2+}$. IR (ν/cm^{-1}): 1177 s (uncoordinated P═O), 1140 s (coordinated P═O). UV-vis (MeCN, 2.3 × 10^{-3} M): λ_{max}/nm (ε/M^{-1} cm^{-1}): 649 (654).

Conclusions

The work reported here presents the first systematic study of the coordination chemistry of triaza and tetraaza macrocycles with neutral phosphine oxide pendant groups, establishing the coordination modes towards a range of divalent late 3d transition metal ions. For the tacn-based ligands $\mathbf{L^1}$ and $\mathbf{L^2}$ it was found that a six-coordinate octahedral geometry was strongly favoured for all the metals; for the pentadentate $\mathbf{L^1}$ the vacant coordination site was occupied by an acetonitrile ligand for all except copper, where instead an O-bound $[Cu(NO_3)_4]^{2-}$ dianionic ligand was preferred over MeCN. For Cu(II) we found that altering the ligand denticity affects the type of Jahn–Teller distortion observed (tetragonal elongation (with $\mathbf{L^1}$) *vs.* tetragonal compression (with $\mathbf{L^2}$)).

The potentially heptadentate cyclen-based ligand, $\mathbf{L^3}$ was found to coordinate in a hexadentate manner forming complexes of the type $[M(\mathbf{L^3})][BPh_4]_2$ (M = Co, Ni, Zn), in which the four amine functions and the two phosphine oxide arms adjacent to the *N*-benzyl group coordinate to the metal ion, leaving the third phosphine oxide which is positioned across the ring from the *N*-Bn group, uncoordinated (N_4O_2 donor set). For the $\mathbf{L^3}$ complexes the geometries are dependent on the metal ion, with cobalt(II) and zinc(II) forming approximately trigonal prismatic dications and the smaller nickel(II) adopting a distorted octahedral geometry. This is consistent with what is seen for the potentially octadentate ligand, **DOTP-Ph**, where the coordination number and geometry is strongly dependent on the choice of metal, although the actual coordination environments observed for $\mathbf{L^3}$ in the present study are markedly different from those reported for **DOTP-Ph**, which binds in an unexpected octadentate manner to Zn(II) and Co(II).[12]

These studies pave the way for a more thorough investigation of the coordination of $\mathbf{L^1}$–$\mathbf{L^3}$ and related derivatives towards Group 1 and 2 metals ions to clarify the speciation of their complexes,[1,2] as well as to probe their suitability for encapsulating larger p- and d-block ions.

Conflicts of interest

There are no conflicts to declare.

Data availability

Original spectra are included in the supplementary information (SI). Supplementary information: comprises full spectroscopic data for all the ligands and complexes described, along with the table of X-ray crystallographic parameters (Table S1) and views of the structures of the additional complexes not shown in the main paper. See DOI: https://doi.org/10.1039/d6dt00255b.

CCDC 2516147–2516157 contain the supplementary crystallographic data for this paper.[19a–k]

Acknowledgements

We thank the EPSRC for support through the Mithras Programme Grant (EP/SO32789/1), as well as GE Healthcare and the EPSRC for a PhD studentship (N. K. S.).

References

1 K. B. Yatsimirskii, E. I. Sinyavskaya, L. V. Tsymbal, T. Y. Medved', B. K. Shcherbakov, Yu. M. Polikarpov and M. I. Kabachnik, *Russ. J. Inorg. Chem.*, 1984, **29**, 512–516.
2 K. B. Yatsimirskii, M. I. Kabachnik, E. I. Sinyavskaya, T. Ya. Medved', Yu. M. Polikarpov and B. K. Shcherbakov, *Russ. J. Inorg. Chem.*, 1984, **29**, 510–512.
3 N. Burford, B. W. Royan, R. E. v H. Spence, T. S. Cameron, A. Linden and R. D. Rogers, *J. Chem. Soc., Dalton Trans.*, 1990, 1521–1528.
4 S. J. Coles, A. P. Hunter, S. J. Fieldhouse, A. M. J. Lees, L. J. McCormick McPherson and A. W. G. Platt, *Polyhedron*, 2025, **269**, 117395.
5 A. W. G. Platt, *Coord. Chem. Rev.*, 2017, **340**, 62–78.
6 A. S. Vijai Anand, S. Perinbanathan, I. Singh, R. R. Panicker, T. Boominathan, A. S. Gokul and A. Sivaramakrishna, *ChemCatChem*, 2024, **16**, e202400844.
7 E. Kukkonen, E. J. Virtanen and J. O. Moilanen, *Molecules*, 2022, **27**, 3465.
8 K. R. Enikeeva, A. V. Shamsieva, A. I. Kasimov, I. A. Litvinov, A. P. Lyubina, A. D. Voloshina, E. I. Musina and A. A. Karasik, *Inorg. Chim. Acta*, 2023, **545**, 121286.
9 A. N. Turanov, V. K. Karandashev and V. E. Baulin, *Solvent Extr. Ion Exch.*, 1996, **14**, 227–245.
10 F. I. Bel'skii, Y. M. Polikarpov and M. I. Kabachnik, *Russ. Chem. Rev.*, 1992, **61**, 221.
11 M. A. Konstantinovskaya, E. I. Sinyavskaya, K. B. Yatsimirskii, B. K. Shcherbakov, Yu. M. Polikarpov, T. Ya. Medved' and M. I. Kabachnik, *Russ. J. Inorg. Chem.*, 1985, **30**, 14631467.
12 E. J. Sinyavskaya, M. A. Konstantinovskaya and K. B. Yatsimirskii, *Russ. J. Inorg. Chem.*, 1987, **32**, 685–688.
13 G. S. Tsebrikova, I. N. Polyakova, V. P. Solov'ev, I. S. Ivanova, I. P. Kalashnikova, G. E. Kodina, V. E. Baulin and A. Yu. Tsivadze, *Inorg. Chim. Acta*, 2018, **478**, 250–259.
14 M. M. Le Roy, S. Héry, N. Saffon-Merceron, C. Platas-Iglesias, T. Troadec and R. Tripier, *Inorg. Chem.*, 2023, **62**, 8112–8122.
15 V. Quint, F. Morlet-Savary, J.-F. Lohier, J. Lalevée, A.-C. Gaumont and S. Lakhdar, *J. Am. Chem. Soc.*, 2016, **138**, 7436–7441.
16 G. M. Sheldrick, *Acta Crystallogr., Sect. A:Found. Adv.*, 2015, **71**, 3–8.
17 G. M. Sheldrick, *Acta Crystallogr., Sect. C:Struct. Chem.*, 2015, **71**, 3–8.
18 O. V. Dolomanov, L. J. Bourhis, R. J. Gildea, J. a. K. Howard and H. Puschmann, *J. Appl. Crystallogr.*, 2009, **42**, 339–341.
19 (*a*) CCDC 2516147: Experimental Crystal Structure Determination, 2026, DOI: 10.5517/ccdc.csd.cc2qg81j; (*b*) CCDC 2516148: Experimental Crystal Structure Determination, 2026, DOI: 10.5517/ccdc.csd.cc2qg82k; (*c*) CCDC 2516149: Experimental Crystal Structure Determination, 2026, DOI: 10.5517/ccdc.csd.cc2qg83l; (*d*) CCDC 2516150: Experimental Crystal Structure Determination, 2026, DOI: 10.5517/ccdc.csd.cc2qg84m; (*e*) CCDC 2516151: Experimental Crystal Structure Determination, 2026, DOI: 10.5517/ccdc.csd.cc2qg85n; (*f*) CCDC 2516152: Experimental Crystal Structure Determination, 2026, DOI: 10.5517/ccdc.csd.cc2qg86p; (*g*) CCDC 2516153: Experimental Crystal Structure Determination, 2026, DOI: 10.5517/ccdc.csd.cc2qg87q; (*h*) CCDC 2516154: Experimental Crystal Structure Determination, 2026, DOI: 10.5517/ccdc.csd.cc2qg88r; (*i*) CCDC 2516155: Experimental Crystal Structure Determination, 2026, DOI: 10.5517/ccdc.csd.cc2qg89s; (*j*) CCDC 2516156: Experimental Crystal Structure Determination, 2026, DOI: 10.5517/ccdc.csd.cc2qg8bt; (*k*) CCDC 2516157: Experimental Crystal Structure Determination, 2026, DOI: 10.5517/ccdc.csd.cc2qg8cv.